Egyptian Journal of Geology

https://egjg.journals.ekb.eg

Mineralogical, fluid inclusion and radiometric studies on Wadi El-Dob pegmatites, northern Eastern Desert, Egypt

Waheed Elwan[1], **Ahmed Dardier**[2], **Ismail A. El Akeed**[2], **Emad Kahlil**[1] and **Hader Sobhy**[1]

[(1)] Geology Department, Faculty of Science, Zagazig University, Zagazig-4451, Egypt
[(2)] Nuclear Materials Authority, P.O. Box – 530 Maadi, Cairo, Egypt

THE WADI El-Dob pegmatite body, located in the northern Eastern Desert, consists of three distinct zones: the border zone, intermediate zone, and core zone. It is hosted within alkali-feldspar granite and contains minerals such as plagioclase, quartz, muscovite, rare K-feldspar, fluorite, topaz, hematite, rutile, pyrite, cassiterite, columbite-tantalite, and xenotime, so they classified as NYF-type pegmatites. Fluid inclusion studies revealed the presence of three types of inclusions: two-phase aqueous, three-phase (H_2O-CO_2), and poly-phase inclusions. The first type (stage I) showed low salinity and homogenization temperature, while the second type (stage II) exhibited high salinity and temperature. The poly-phase inclusions formed during the hydrothermal stage. The wide temperature range of homogenization could be attributed to simple cooling. The estimated temperatures from isochors varied between a lower and upper range under a specific pressure. The fluids of both stages I and II likely originated from a magmatic source, possibly associated with the devolatilization of alkali-feldspar granites. The coexistence of different types of inclusions can be explained by the partial immiscibility of a homogeneous fluid (H_2O-CO_2-NaCl) due to the presence of H_2O-rich and CO_2-rich inclusions, their occurrence in the same region and samples, and the similar micro thermometric results. Generally, pegmatites are commonly suggested to be derived from crystallizing granitic melt especially those pegmatites, which are hosted within the parental granite. Geochemically, the resemblance of magma type between alkali-feldspar granites and the associated pegmatite body suggests a common source magma. Both granite and pegmatite samples display a typical trend of magmatic differentiation, which is consistent with fractional crystallization. NYF, garnet-REE pegmatite containing ilmenite and Nb-Ta minerals may originate as the product of melt segregation within the granite during its crystallization. Furthermore, NYF pegmatites may have originated from mantle-sourced anorogenic magmas with a peralkaline signature. The border zone of the pegmatite experienced crystallization temperatures within a range (560 - 570 °C). The chemical composition of the intermediate zone (K-feldspar) from Wadi El-Dob and the physical tests conducted on ceramics made from pegmatite samples indicate their suitability for wall ceramic tiles according to standard values. Field radiometric measurements of the El Dob pegmatites revealed varying content of K-40, uranium, and thorium. These variations indicate the presence of hydrothermal and magmatic types, suggesting significant post-magmatic processes. Consequently, it is recommended to exclude measurement stations with high values from use in the ceramic industry.

Keywords: Pegmatite, Eastern Desert, Fluid inclusions, El-Dob, Heavy minerals, Radiometry, Ceramic.

1. Introduction

Pegmatites considered as coarse to very coarse-grained granites. They represent an important source of industrial minerals (feldspars, quartz, spodumene, petalite), hi-tech mineral commodities (e.g., Li, Cs, Be, Nb, Ta, Sn), radioactive minerals (e.g., Th and U), and gemstones (Pal et al., 2007; Simmons et al., 2006; Vasyukova and Williams-Jones, 2019). Pegmatite bodies vary greatly in size and shape; their shapes range from pockets, dykes, sheets to huge plugs. Pegmatites in a particular field may show a regional mineralogical-chemical zonation (Černy, 1982). Rare metal-bearing pegmatites are classified into two petrogenetic families based on accessory phase mineralogy and

*Corresponding author e-mail: wielwan@science.zu.edu.eg
Received: 13/07/2023; Accepted: 16/08/2023
DOI: 10.21608/EGJG.2023.221581.1053

their rare metal enrichment trends (Černy, 1991a, b). The LCT family is characterized by enrichment in Li, Cs, Ta, while NYF family is marked by enrichment in Nb, Y, F.

Pegmatites are widely distributed in the northern portion of the Egyptian Eastern Desert, and they found throughout different types of the country rocks (Fawzy et al., 2020). Most pegmatites are cogenetically related to the younger granites. Generally, most acidic pegmatites have granitic composition. Few pegmatite bodies are incorporated with mafic-ultramafic rocks. Barren pegmatites are widely scattered as mono-veins or dykes in various country rocks at various areas all over the Egyptian Eastern Desert, whereas zoned and mineralized pegmatites bodies are rare.

Pegmatites vary in length, width, and direction. They are penetrated and/or invaded migmatite-gneiss, gneiss, granodiorite, tonalite, trondhjemite and alkali granites. Four pegmatites field can be recognized in the Eastern Desert of Egypt (El Shazly et al, 1974; Greenberg, 1981; Rashwan, 1991; Khaleal et al., 2022) namely:

1. Gattar –Wadi Hebal pegmatite field, that located at the northern portion of Eastern Desert. Molybdenum, REE, and fluorite-bearing pegmatites are observed at Gabal Gattar (Shalaby et al., 1999; El-Nahas, 1997) and Abu Zawal area (Helmy, 1999).

2. Wadi Bezah pegmatite field, that located at the central portion of the Eastern Desert. Beryl, mica, Sn, Nb, Ta, REEs, and fluorite bearing pegmatites are observed at different areas (e.g., Nweibia, Abu-Dabba, lgla, Mueiha, Homrit Waggat, and Wadi Bazih).

3. Migif-Hafafit pegmatite field that lies between the central and southern parts of Eastern Desert. Corundum, emerald/beryl, vermiculite, asbestos, mica Nb, Ta, and fluorite beaning pegmatites are observed at various areas (e.g., Nugrus, Sikait, Zabara, Hafafit-Migif, Umm Kabo, Abu-Rasheid, and Abut Nimr).

4. Umm Rasein-Hamaany pegmatite field, which located at Southern portion of the Eastern Desert. This field is characterized by mica and tourmaline mineralization (e,g. Umm Rasein, Umm Tayor, Wadi Umm Hebal area around sol Hamid shear zone and Garf).

From economic and metallogenic point of views, the boundary zone between the central and southern portions of the Eastern Desert is the most important zone, where huge pegmatite fields are extending around Migif-Hafafit terrain (Khaleal et al., 2022). NYF-pegmatites are recorded at Kadabora (Saleh, 2007), Ras Baroud (Raslan et al., 2010a; Fawzy et al., 2020), Wadi Khuda (Raslan et al., 2010b), Abu Rusheid (Raslan and Ali, 2011), and Gabal El Faliq (Abu Elatta, 2019).

Abdel Ghani (2001) described Wadi El-Dob pegmatites as simple zoned pegmatites, which are hosted in perthitic leucogranites and quartz diorites. Khaleal (2014) separated Wadi El-Dob pegmatite zones into an outer zone that envelope an inner core of quartz.

Fluid inclusion study is one of valuable tools in the understanding of late-magmatic and hydrothermal processes (Abd El Monsef et al, 2023). Fluid inclusions can provide indispensable information about the environments and geologic processes in which the minerals were formed, particularly the composition, temperature, and pressure of the geofluids (Hollister & Crawford, 1981). The radiometric investigation was performed for two target**s**. The first one aims to determine the pegmatites contents from radioactive elements ^{40}K, uranium and thorium. The second target, due to estimated results, will be delineate the environmental safety agreeability of using this pegmatite in ceramic industry.

The aim of the present article is to investigate the petrological, mineralogical, and geochemical characteristics of Wadi El-Dob pegmatite bodies as well as their fluid inclusions petrography, test their suitability for ceramic industry and their radiometric hazards.

2. Geologic background

Wadi El-Dob area located in the northern Eastern Desert of Egypt just south Hurghada - Suhage paved road at 33 km from its intersection with Safaga-Qena paved road. It is located between latitudes 26^{o} 44\` 59\`\`N and between longitudes 33$^{o}$ 25\` 52\`\` E (Fig.1a). The area is characterized by the presence of moderate to high relief mountains. The area is covered by rock units arranged from the oldest to the youngest into older granite, Dokhan volcanics, younger gabbros (i.e. fresh gabbro not metagabbros), alkali-feldspar granite and pegmatite bodies. Wadi El-Dob pegmatites are hosted in alkali feldspar granites (Fig.1b). Alkali feldspar granites form an oval to circular outlines hills. They are coarse-grained rock with yellowish pink color. The contact between alkali-feldspar granites and the associated pegmatite body is sharp intrusive contacts. The main pegmatite body is zoned with an oval-shaped outline (Fig.1c). This pegmatitic body is trending in NE – SW direction that almost parallel to the contact zone. It is subjected to quarrying processes and the rest of this body has 110 m length and 50 m breadth.

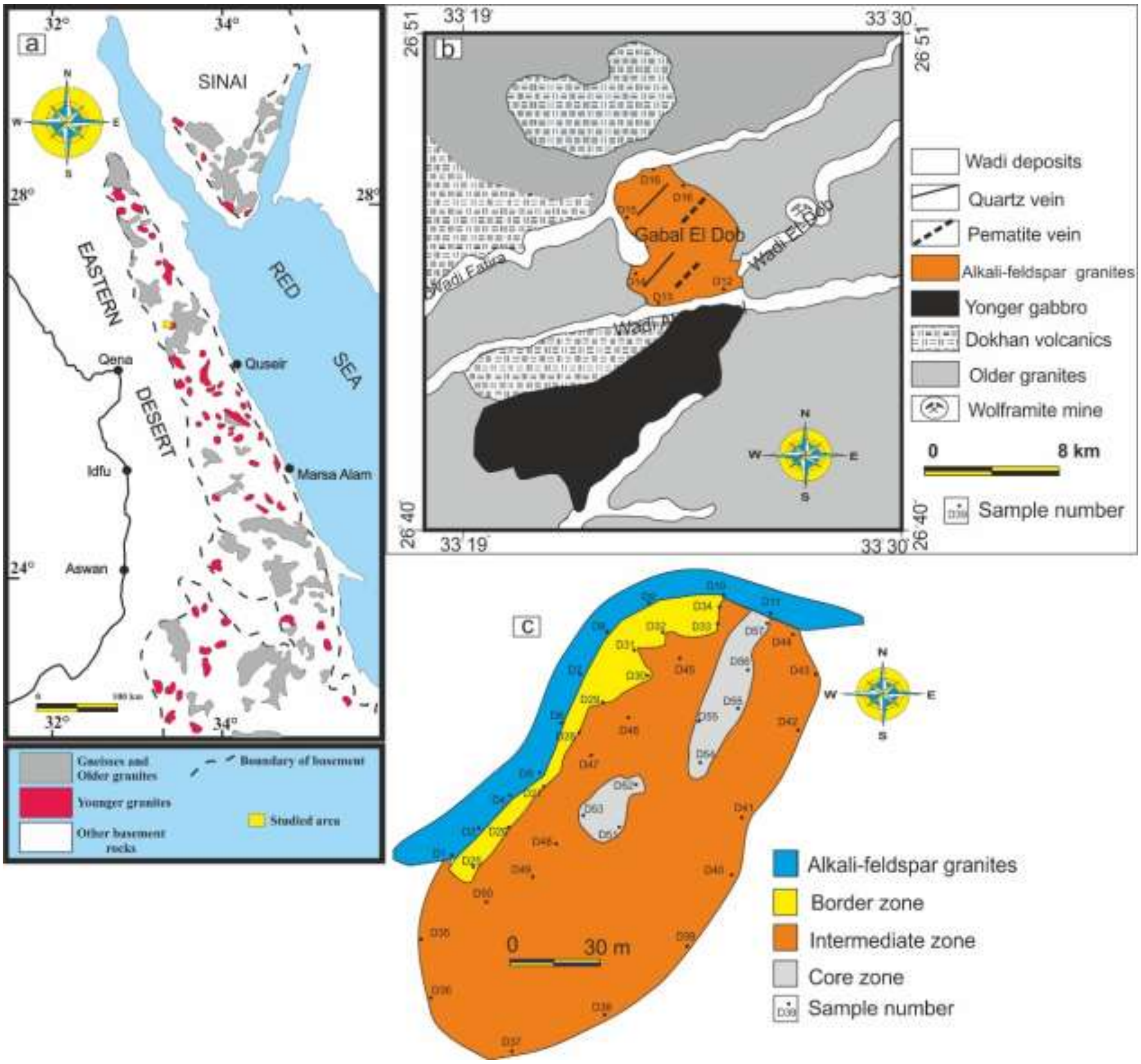

Fig. 1. a) Distribution of granitic rocks and pegmatite bodies in the Eastern Desert and Sinai (Greenberg, 1981) for the Eastern Desert and El-Shazly et al. (1974) for Sinai Peninsula); b) Geologic map of Wadi El-Dob area and c) Sketch shows zoned pegmatite body of Wadi El-Dob area.

The zoned pegmatite body consists of the three successive zones: a) border zone is the outer zone, which consists of 8-15 cm discontinuous aplite (fine graine granites; Fig.2a & b; Fig. 3a). It consists mainly of plagioclase, quartz, muscovite and rare feldspar and fluorite (Fig.3b). K-feldspar increases gradually towards the intermediate zone.; b) Intermediate zone, which forms the main constituent of the pegmatite body, and it consists of blocky K-feldspars (Fig.2c). It consists mainly of perthite, quartz and muscovite. The color of K-feldspars has changed to brick-red due to ferrugination process (Fig.2d; Fig. 3b), at which the K-feldspar and quartz phenocrysts are partially devitrified glassy groundmass and totally ferruginated with hematite. Mn-dendrites are commonly recorded along joint planes (Fig.3c); c) core zone, which consists of amoeboid-shape quartz. This quartz is commonly enclosing isolated flakes and/or nests of muscovite (Fig.3d) and rarely biotite and opaques (Fig.3e). Quartz is of milky color (Fig.2e), but it contains joints and fractures, which are commonly stained with iron hydroxides (Fig.2f & Fig.3f).

3. Analytical techniques

More than 50 samples were collected from the granites and associated zoned pegmatite bodies for petrographical study. The heavy mineral separation, the Scanning Electron Microscope (SEM) investigation of separated minerals and the radiometric study were carried out at Nuclear Material Authority Laboratories. For the mineralogical separation using bromoform to concentrate the heavy minerals and then the heavy minerals were picked under binocular microscope. The mineralogical investigation carried out using SEM model (PHILIPS XL 30) attached with Energy Dispersive X-ray unit (EDX). The microanalyzer worked out at an operating voltage of 25 KV, 1-2mm diameter, 60-120 second counting time and high-resolution backscattered electron images (BSE) with using ZAF correction errors. For the radiometric study, the measurements of the radioactive elements distribution and concentration were performed using the portable gamma-ray spectrometer Gs 512 instrument. The chemical analyses of border zone (i.e. 3 samples) and intermediate zone or K-feldspar (1 sample) were carried out for powder (<74 μm) samples using X- Ray fluorescence (XRF) equipment Philips PW2404 with eight analysing crystals and maximum power of the equipment was 30 K.wt., Crystals (LIF-200), (LIF-220). at the Central Laboratories of Egyptian Mineral Resources General Authority (EMRA), Dokki, Cairo, Egypt. The fluid inclusion petrography and microthermometric measurements were carried out on 3 doubly polished wafers quartz samples 0.2-0.3 mm thick using a Chaixmeca heating freezing stage (Poty et al., 1976) at Geology Department, Assiute University. The stage was calibrated for temperatures between -100 and 400℃ using Merck chemical standards as well as according to the melting point of distilled water (0 ℃) and phase transition in natural pure CO_2 inclusions with triple point (56.6 ℃). From microthermometric results the bulk composition and density of the fluids could be calculated by using the equation of state of Zang & Frantz (1987) for the H_2O- NaCl system, and Bowers and Helgeson (1983) for volatile rich system. Isochores for different fluid densities are calculated until a fit with the known homogenization temperature is achieved using the Flincor computer program (Brown, 1998). The minimum pressure of trapping is estimated from the constructed P-T diagrams. The physical parameters tests on the prepared green biscuit samples from intermediate zone. The prepared green ceramic samples are 5 cm in width and 10 cm in length with 1.52 cm thickness. They pressed using SACMI imola presser. Each green ceramic sample was dried and fired, then shrinkage testing was carried out using Vernier caliper 150 x 0.05 mm. Shrinkage is the rate of change in length and width for inspection sample. Samples were subjected to stress testing for measuring the bending stress by using Gabbrielli Crometro CR5 instrument. Finally, the water absorption was measured for each sample. These tests were carried out in the Laboratories of Arab Contractors Company.

4. Results

4.1. Petrography

4.1.1. Alkali-feldspar granite

Alkali-feldspar granites are coarse-grained rocks that display hypidiomorphic texture with pinkish color. They are composed mainly of K-feldspars (perthite and orthoclase-perthite) up to 53%, quartz up to 15% and plagioclase up to 25% with rare biotite. Muscovite and chlorite after biotite are found as secondary minerals. Iron oxides, allanite, sphene, zircon, monazite, apatite, and are the main accessory minerals.

Perthite occurs as subhedral phenocryst and it forms veins, veinlet, and patchy types perthite (Fig.4a &b). Orthoclase- perthite occur as subhedral crystals, which rarely show clear simple twinning due to perthitization. Quartz varies in size from fine to coarse subhedral to anhedral grains. Fine-grained quartz is filling the interstitial spaces between feldspar minerals (Fig.4b). Euhedral crystals of quartz are recorded within perthitized K-feldspar suggesting that quartz is an early crystallized phase (i.e. high temperature quartz). Plagioclase found as two generations; the first one occurs as subhedral and platy crystals (Fig.4c), while the second has an exsolved origin with albite composition. The latter phase is muscovite.

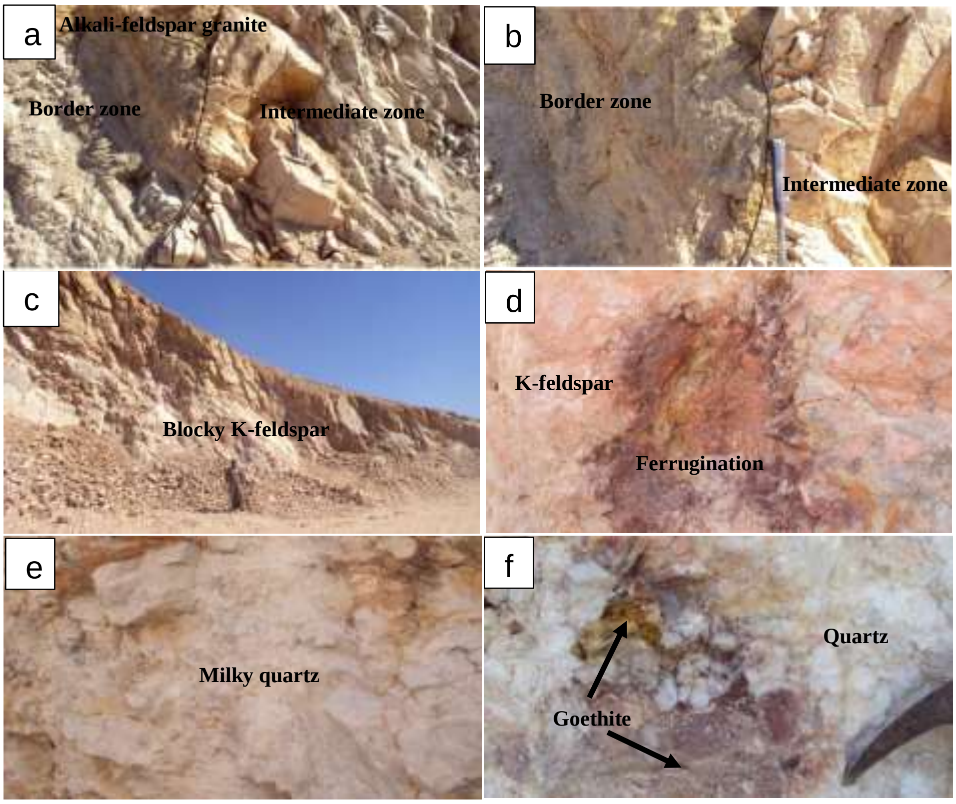

Fig. 2. a) Contact between alkali-feldspar granites, border and intermediate zones, Wadi El-Dob pegmatite body; b) Contact between border zone and intermediate zone; c) K-feldspar forming the main constituent of the intermediate zone d) Ferrugination of K-feldspar in the intermediate zone; e) Milky quartz in core zone; f) Iron oxy-hydroxides in quartz core.

Biotite is very rare and found as subhedral to anhedral minute flacks. They are partially or completely altered to muscovite and/or chlorite. Muscovite occurs as either as subhedral flacks after biotite or as minute crystals after plagioclase. Chlorite formed after biotite with anomalous blue or violet interference color. Allanite found a subhedral crystals (Fig. 4b), which are commonly show metamictization along their cores due to radiation effects, where metamectic cores are sending anastomosing cracks along surrounding minerals. Sphene occurs as subhedral to euhedral spindle shape crystals, which are associated with iron oxides and zircon. Zircon occurs as subhedral to euhedral crystals. Monazite occurs as subhedral minute crystals associated with zircon and apatite. Apatite occurs as colourless euhedral needle-shape crystals. Iron oxides are found along grains boundaries between perthite crystals (Fig. 4a). Plagioclase is partially altered to sericite and represented by magnetite and ilmenite. Goethite is common and shows colloform texture (Fig. 4d).

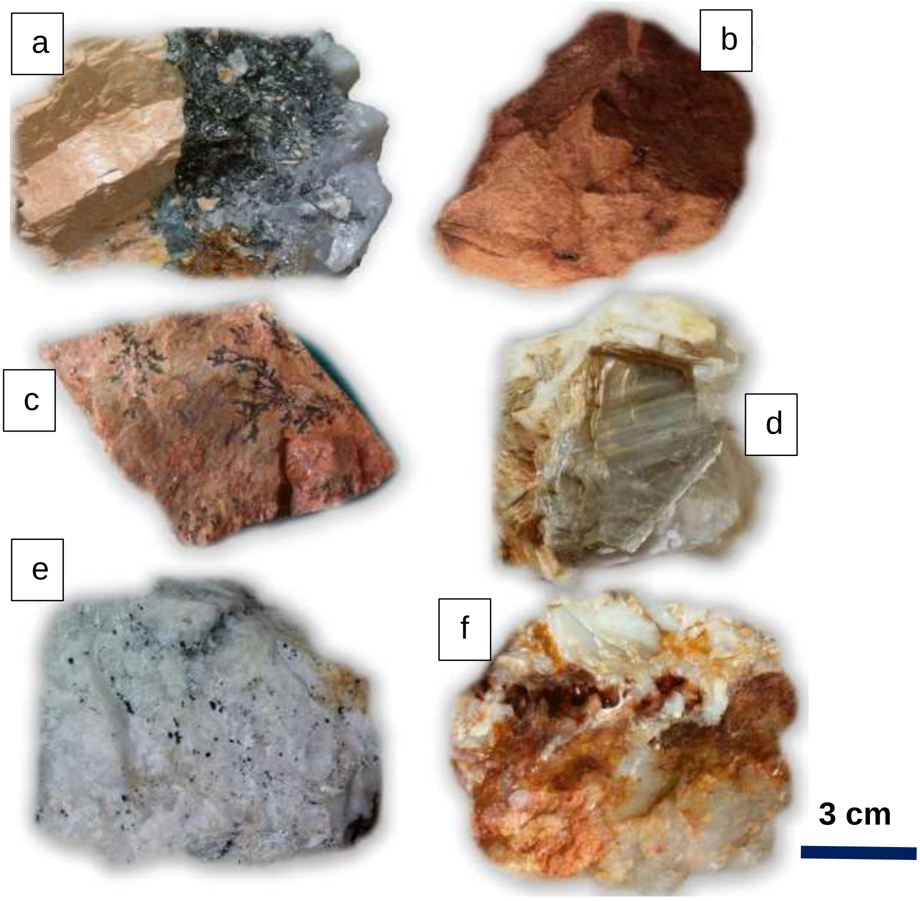

Fig. 3. Characteristic features of hand specimens of Wadi El-Dob pegmatites, a) K-feldspar and biotite, border zone; b) Brick-red K-feldspar, intermediate zone; c) Mn–dendrites in K-feldspar, intermediate zone; d) Isolated flakes of muscovite, core zone; e) Quartz with rarely biotite and opaque minerals, core zone; f) Quartz stained with iron oxy-hydroxides, core zone.

4.1.2. Zoned pegmatites

Zoned pegmatite body is composed of three succussive zones as follow:

a) The border zone has granitic composition, and it consists mainly of plagioclase, quartz, muscovite, and rare K-feldspar with subordinate amount of fluorite and topaz. Plagioclase is found along grains boundaries between perthite crystals and partially altered to sericite and muscovite (Fig.4e). Quartz forms subhedral to anhedral fine to coarse-grained grains. Iron-oxides are represented by magnetite and ilmenite.

b) Intermediate zone is consisting mainly of perthite, quartz and muscovite. Perthite shows string braided and patchy-types perthite. Quartz forms subhedral to anhedral crystals, which corrode the perthite (Fig 4f) and muscovite. Muscovite occurs either as subhedral prismatic lathes, or as fine inclusion within perthite phenocrysts. Magnetite and ilmenite are iron-oxide minerals.

c) Core zone is composed mainly of quartz. Quartz crystals vary in size and shape, and they occur either as fine rod-like grains or very coarse subhedral to anhedral phenocrysts. Sometimes, quartz grains enclose isolated flakes and /or nests of muscovite. Inclusion of columbite-tantalite minerals cassiterite grains (Fig.4g & h) are common either within quartz or enclosed within muscovite nests. Cassiterite occurs as subhedral zoned grains showing elbow twining (Fig.4g). columbite-tantalite occurs euhedral long prismatic grains (Fig.4h). The presence of columbite-tantalite, cassiterite and fluorite is indicating that El-Dob pegmatite body may classified as NYF type pegmatites.

4.3. Heavy minerals

The minerals in heavy mineral separates are include hematite goethite, zircon and pyrite. Hematite [Fe_2O_3] and goethite [FeO (OH)] are medium to coarse compact grains with brownish-red, bright yellow and dark brown color (Fig.5a & b), which were separated at 0.2 and 0.5 ampere fractions. Hematite and goethite mainly originated from alteration of magnetite and pyrite. Zircon [$ZrSiO_4$] forms euhedral to subhedral grains with colourless, honey yellow and red color (Fig.5c). It is preserved as long and short prismatic crystals, while few of zircon crystals have bipyramidal termination. Zircon is rare and is restricted in 1.0, ampere non-magnetic fractions depending on iron-oxides staining and type of inclusions.

Pyrite [FeS_2] is present in a considerable amount in Wadi El-Dob pegmatites (exactly, within 1.5 ampere nonmagnetic fraction). It occurs as subhedral to anhedral brass golden yellow to dark brown color (Fig.5d). It contains traces of Ca and is composed mainly of S and Fe. Pyrite is commonly altered to iron oxyhydroxides that shows reddish and yellowish tint. The investigated minerals by scanning electron microscope include xenotime, pyrite and cassiterite. Xenotime [YPO_4] occurs as inclusions in quartz and feldspars (Fig.6a) within 0.5 ampere magnetic fraction. The EDAX analysis data show that the studied xenotime is contain SiO_2 with no U_2O_3 and CaO. The major components of xenotime are Yttrium (Y) and P, while REE (i.e. Dy, Er and Yb) are the

secondary components. On the other hand, Si, Al, Mg and K oxides occur as trace impurities. Xenotime is the most common mineral containing predominantly yttrium and the HREEs.

Cassiterite [SnO_2] occurs as bright isolated grains (Fig.6b) and/or as inclusions within feldspars. It is separated exactly, within 1.5 ampere magnetic fraction. It contains traces of Si and Ca and it composed mainly of Sn.

(Fig.5a & b), which were separated at 0.2 and 0.5 ampere fractions. Hematite and goethite mainly originated from alteration of magnetite and pyrite. Zircon [$ZrSiO_4$] forms euhedral to subhedral grains with colourless, honey yellow and red color (Fig.5c). It is preserved as long and short prismatic crystals, while few of zircon crystals have bipyramidal termination. Zircon is rare and is restricted in 1.0, ampere non-magnetic fractions depending on iron-oxides staining and type of inclusions.

Pyrite [FeS_2] is present in a considerable amount in Wadi El-Dob pegmatites (exactly, within 1.5 ampere nonmagnetic fraction). It occurs as subhedral to anhedral brass golden yellow to dark brown color (Fig.5d). It contains traces of Ca and is composed mainly of S and Fe. Pyrite is commonly altered to iron oxyhydroxides that shows reddish and yellowish tint. The investigated minerals by scanning electron microscope include xenotime, pyrite and cassiterite. Xenotime [YPO_4] occurs as inclusions in quartz and feldspars (Fig.6a) within 0.5 ampere magnetic fraction. The EDAX analysis data show that the studied xenotime is contain SiO_2 with no U_2O_3 and CaO. The major components of xenotime are Yttrium (Y) and P, while REE (i.e. Dy, Er and Yb) are the secondary components. On the other hand, Si, Al, Mg and K oxides occur as trace impurities. Xenotime is the most common mineral containing predominantly yttrium and the HREEs.

Cassiterite [SnO_2] occurs as bright isolated grains (Fig.6b) and/or as inclusions within feldspars. It is separated exactly, within 1.5 ampere magnetic fraction. It contains traces of Si and Ca and it composed mainly of Sn.

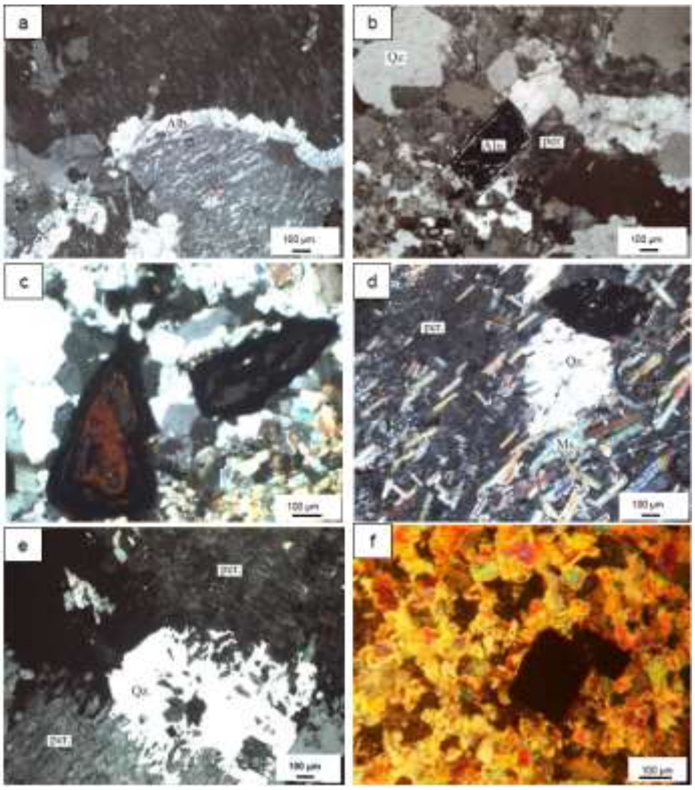

Fig. 3. a) Albite (Alb) bands separating two perthite crystals in the alkali-feldspar granites, CN, b) Euhedral allanite (Aln) crystal enclosed within perthite (per) crystal in the alkali-feldspar granites, CN, c) Magnetite hydrated into goethite, which shows colloform texture and surrounded by quartz and muscovite in the alkali-feldspar granites, CN, d) Quartz (Qz) and prismatic lathes of muscovite (Ms) in border zone of the pegmatite body, CN, e) Quartz (Qz) grain corroded both of perthite (Per) and muscovite in intermediate zone of the pegmatite body, CN and f) Cassiterite (Cs) and columbite-tantalite (CT) grains surrounded by muscovite groundmass, CN.

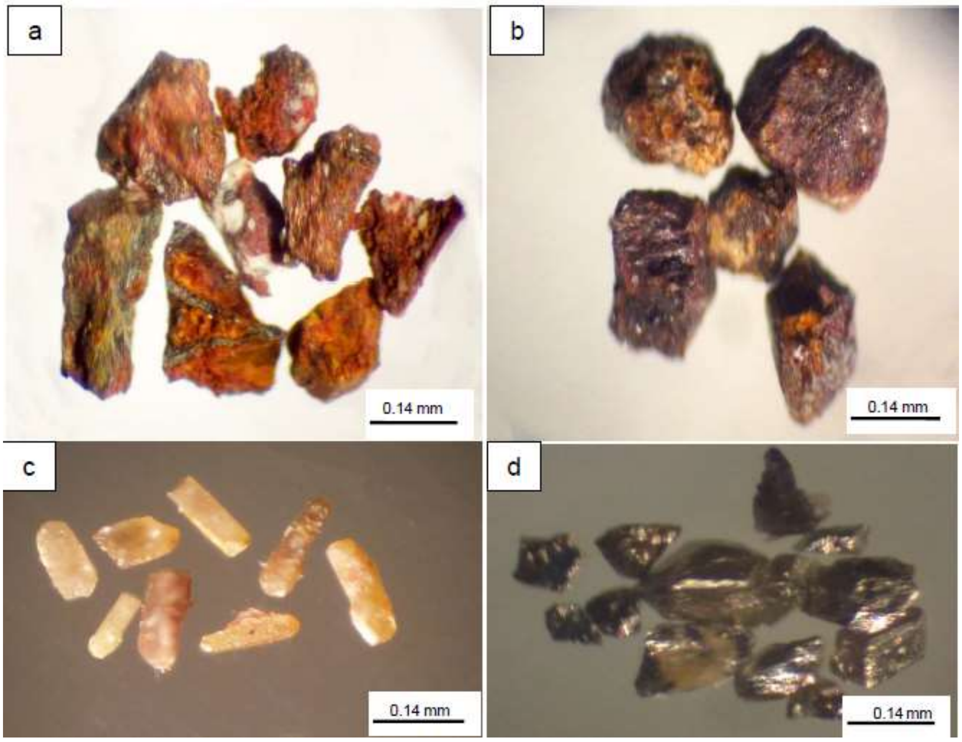

Fig. 5. Photomicrographs showing of separated minerals from Wadi El-Dob pegmatite body a) Hematite with bright red color with irregular quartz veinlets; b) Hematite with dark brown color with several dark yellow goethite patches; c) Subhedral to euhedral zircon grains usually stained with iron oxides, within 1.0 ampere magnetic fraction; d) Subhedral to anhedral pyrite grains with dark brown color, within 1.5 ampere nonmagnetic fraction.

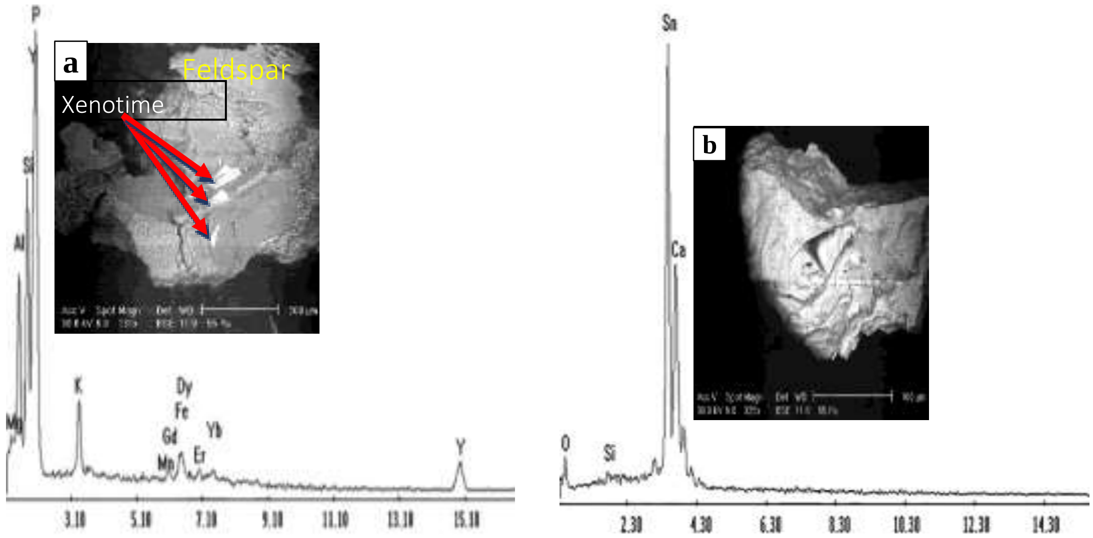

Fig. 6. BSE images, and EDAX charts show a) Xenotime overgrowth feldspar crystal; b) Cassiterite grain, Wadi El-Dob pegmatites, Z: error in atomic No., A: error in atomic weight and F: error in fluorescence signal intensity.

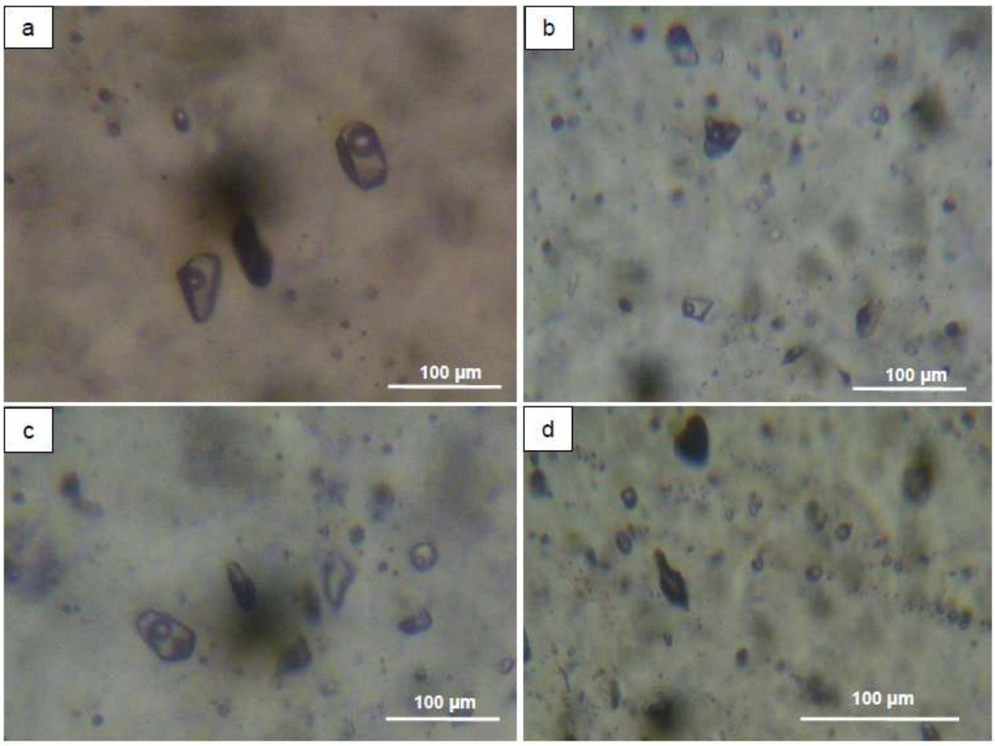

Fig.7. Photomicrograph showing, a) Primary distribution as individual isolated inclusions of two phase aqueous, Wadi El-Dob area; b) Primary distribution of two phase aqueous in three directions; c) Coexistence of primary distribution of three phase (H_2O- CO_2) inclusions (subtype1b); d) Distribution of secondary inclusions of type 2.

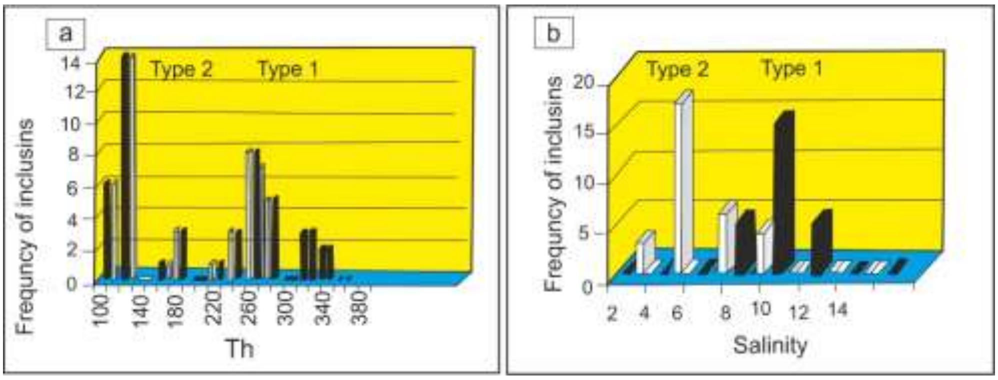

Fig. 8. Histogram showing the microthermometric (Th and Salinity) frequency distribution in the studied pegmatites: a and b) Frequency distribution of homogenization temperature (Th) and salinity respectively in Wadi El-Dob pegmatite.

4.4. Fluid inclusions

Fluid inclusions are tiny cavities containing liquid, gas and/or solids. These fluids trapped in quartz can either represent fluid from cooling magma (i.e. primary) or later fluids developed during hydrothermal stages (i.e. secondary). Both types of fluids developed may be trapped in apparently unaltered samples of rock (Roedder, 1979). The primary inclusions were trapped during the growth of their surrounding host crystals and occur as isolated groups, sometimes confined within growth zone of quartz, while secondary fluid inclusions are related to fractures and/or cleavage planes. Three doubly polished samples from quartz core of Wadi El-Dob pegmatite body were studied for fluid inclusions.

4.4.1. Fluid inclusion petrography

Fluid inclusion petrographic investigations in quartz of El-dob pegmatite samples recorded the following inclusion types:

4.4.1.1. Primary inclusions

Primary inclusions include two subtypes, which are:

a) Subtype 1a: Two phase (L+V) aqueous inclusions. They are easily recognizable by their clear appearance (Roedder, 1984). They are distributed either as individual isolated inclusions (Fig. 7a) and/or in three dimensions (Fig. 7b). These inclusions show rounded, oval, negative-crystal, and triangular to elongated shapes. Their sizes range from 10 to 20 µm with vapor phase range between 10- 30% of the total volume of the inclusion.

b) Subtype 1b: Three phases (H_2O liquid + CO_2 liquid + CO_2 vapor) inclusions (Fig.7b). These inclusions coexist with the subtype 1a aqueous inclusions (Fig.7c). Subtype 1b is characterized by different degrees of fill with CO_2 contents ranging from 0.3 to 0.9 of the total volume of inclusion.

4.4.1.2. Secondary inclusions

Secondary inclusions distributed as lines or fluid inclusion planes along microfractures in quartz crystals (Fig.7d). They are represented mainly by liquid rich two-phase aqueous inclusions in association with poly-phase (L+V+S) inclusions and mono-phase inclusions.

a) Liquid rich two-phase (L+V) aqueous inclusions are characterized by a small size up to 10 µm with vapor phase representing ~ 10 - 30 % of the total volume of inclusions. The shape of inclusions varies from oval, subrounded, triangular and elongated.

b) Poly-phase (L+V+S) inclusions are rare but presently coexisting with liquid rich two-phase aqueous inclusions. The solid phase forms cubic-shape crystals and its size up to 1 µm, which probably represented by halite and sylvite as daughter crystals.

c) Mono-phase inclusions are represented by mono-phase liquid and mono-phase vapor associated with the above-mentioned types of secondary inclusions. The shape of these inclusions is varied from oval, triangular to irregular shape, and the size reaches in some inclusions to 2.0 µm.

4.4.2. Microthermometric measurements

4.4.2.1. Primary inclusions

a) Subtype 1a, two-phase (L+V) aqueous inclusions. Freezing runs to – 90 oC followed by heating one enables us to record melting temperature (Te). As shown in table (1) the eutectic temperature was observed in some inclusions at temperature between -26 ^{o}C and -22 ^{o}C, indicating that NaCl and KCl are the main dissolved salts in the fluid (Borisenko, 1997; Crawford, 1981). The temperature of homogenization (Th) is the temperature at which the gas bubble disappears. These temperatures reached by the disappearance of the vapor bubble at temperature between 160 ^{o}C- 270 ^{o}C, with the majority at 250 ^{o}C (Fig.8a). The final temperature of melting ice (T_{ice}). enables calculations of fluid inclusion salinities. The final melting of ice (Tm_{ice}) was achieved at temperatures between -5 ^{o}C and -3 ^{o}C, corresponding to salinity between 4.96 and 7.86 wt. % NaCl eq. (Bodnar, 1993), with majority at 7 wt. % NaCl eq. (Fig.8b).

b) Subtype 1b, three phase (H_2O-CO_2) inclusions The final melting of solid CO_2 (Tm_{CO2}) is measure of the purity of the phase. Pure CO_2 melts at -56.6 ^{o}C is the triple point of CO_2. Addition of other gases such as CH_4, N_2, H_2S and SO_2 result in depression of this triple point. All measured inclusions have CO_2 melting temperature between -56 ^{o}C and -56.7 ^{o}C, very near to the triple of pure CO_2. This confirms that the phase is CO_2 at ambient temperature, the aqueous fluid and CO_2 phases are completely immiscible, but cooling there is strong interaction between them to form gas hydrates (clathrates) which disturb the behaviour of the remaining aqueous and non-aqueous phases.

The temperature of last clathrate melting (Tm_{clat}.) can give an estimate of the salinity (Collins, 1979; Diamond, 1992). In the studied samples, $Tm_{clat.}$ ranges from 3.3 to 8, giving a salinity estimate between 7.45 to 11.65 wt % NaCl eq., with maximum peak at 10 wt % NaCl eq. (Fig. 8a). In the measured inclusions, the CO_2 phases were homogenized either to liquid or vapor. In the case of homogenization to liquid, the temperatures of homogenization ($Thco_2$) were achieved between 21 ^{o}C to 24 ^{o}C, giving densities of CO_2 between 0.726 to 0.763 g/cm^3 (Shepherd et al., 1985).

In the case of homogenization to vapor the temperature of CO_2 homogenization (Th_{CO2}) measured between 28 ^{o}C and 29 ^{o}C, corresponding to densities of CO_2 between 0.289 and 0.312 g/cm^3.The bulk homogenization temperature (Th_{bulk}) fixes the bulk density of the fluid. In type inclusions, the bulk homogenization temperatures (Th_{bulk}) range from 170 ^{o}C to 340 ^{o}C, with maximum peaks at 260 ^{o}C. Plots of alkali-feldspar granite and associated pegmatites samples show curved trend on Al_2O_3/TiO_2- TiO_2 diagram, which represent an obvious trend of magmatic differentiation (Garcia et al., 1994). This trend is compatible with the fractional crystallization model in Wadi El-Dob area (Fig. 9b). Accordingly, the studied pegmatites were formed from same magmatic source of the country alkali-feldspar granites by fractional crystallization. Furthermore, the crystallization temperatures of the border zone in the studied pegmatite body were calculated according to rutile saturation (Ryerson & Watson, 1987; Hayden & Watson, 2007). They range from 560 °C to 570 °C (Table 2).

Table 1. Microthermometric results in quartz of Wadi El-Dob pegmatites.

Fluid Inclusion type		Measurements
1. Two- phase (L+V) aqueous Inclusions.		
	Th_{tot} (°C):	95 to 270°C
	T_{mice}:	-5 to -1°C
	Salinity in wt% NaCl eq.:	1.47 to 7.86
	T_e (°C):	-22°C
Distributon:		Primary and Secondary
2. Three-phase (H_2O-CO_2) inclusions.		
	$T_{h(tot)}$:	170 to 450°C
	Salinity:	3.9 to 19.1
	$T_{mclat.CO2}$:	-4.6 to 8°C
	Degree of filling:	0.3 to 0.9
	$T_{mCO2:}$	-56.5to-55.8°C
	T_{hCO2} to vapour:	21 to 28°C
	T_{hCO2} to liquid:	28 to 29°C
	d_{CO2}(g/cm^3):	0.77
	d bulk(g/cm^3):	0.82 to 1.13
	Distribution:	Primary
3. Poly-phase (L-V-S) inclusions.		
	T_s:	440-450
		Secondary
	Distribution:	

Table 2. Major element concentration (wt.%) of alkali-feldspar granites, border, and intermediate zones of Wadi El-Dob pegmatites compared with Ceramica Cleopatra Company standard limits.

Locality	Wadi El-Dob					Standard Ceramic raw material	
Rock type	Alkali- feldspar granites Av. (7) *	Border zone			Intermediate zone		
Oxides		D17	D32	D34	D35	From	to
SiO_2	74.1	72.72	83.61	84.95	70.20	68	78max.
TiO_2	0.08	0.01	0.01	0.01	0.01	0	0.1
Al_2O_3	13.0	16.33	10.05	9.32	16.47	11	16
Fe_2O_3	1.54	0.46	0.13	0.15	0.05	0	2max.
MnO	0.02	0.01	0.01	0.01	0.01	0	0.5
MgO	0.21	0.01	0.01	0.01	0.01	0	1max.
CaO	0.31	0.01	0.14	0.01	0.01	0	1max.
Na_2O	4.46	5.43	5.05	3.35	2.74	1	4
K_2O	4.75	3.81	0.32	0.91	9.97	4% min..	over
P_2O_5	0.09	0.01	0.01	0.01	0.01	0	0.5
Cl	-	0.01	0.01	0.01	0.01	-	-
L.O.I	1.07	0.95	0.68	0.97	0.28	-	-
Total	99.70	99.71	99.63	100.03	99.43		
	Normative minerals						
Qz	29.26	26.64	52.83	62.07	16.19		
Or	28.07	22.52	1.89	5.38	58.92		
Ab	37.74	46.799	42.58	28.199	23.037		
An	0.95	0.001	0.63	0.001	0.003		
C	0.17	3.3	1.19	2.85	1.20		
Il	0.04	0.02	0.02	0.02	0.02		
Hem	1.54	0.46	0.13	0.15	0.05		
Ap	0.21	0.02	0.02	0.02	0.02		
$T_{R\text{-}Sat.}$ °C**	-	565.4	567	571.4	-		

*Average of alkali-feldspar granites analyses after (Khaleal, 2014); ** T R-Sat. °C Temperature of crystallization calculated by rutile saturation (Ryerson & Watson, 1987; Hayden & Watson, 2007)

Table 3. The ceramic physical parameters for the tested samples compared with standard limits (Knota, 1980).

Physical parameter	D 35	**Standard limits** (Knota, 1980)	
		Floor	**Wall**
Shrinkage %	14.3%	<3%	14-17%
Bending stress	35	>27.5 Newtons/cm^2	>17 Newtons/cm^2
Water absorption %	5.3%	0-3%	5-6.5%

Table 4. 40K%, eU, eTh (ppm) average contents, maximum, minimum values and eTh/eU ratios of the studied pegmatites.

S. No.	eU (ppm)	eTh (ppm)	eTh /eU
1	16.14	42	5.77
2	4.0	18	3.5
3	5.0	18-20	4
4	0.04-19.7	---------	--------
5	3.0	17	5-7
6	1-6	1-25	2-6

1-Average of the studied pegmatites; 2- Average of granites 77% SiO2 (Rogers & Adams, 1969); 3- Average of the granitic rocks (Clarck et al., 1966); 4- Average of the Alkali intrusive rocks (Clarck et al., 1966); 5- Average of the low Ca-granites (Turkian & Wedepohl, 1961) 6- Average of the acidic intrusive (Adams et al., 1956).

Table 5. ^{40}K%, U, Th (ppm) average contents, ranges and Th/U ratios of the studied pegmatites compared with some published works.

Rock types	Parameters	^{40}K (%)	eU (ppm)	eTh (ppm)	eTh /eU
Pegmatites	Max.	6.9	161.3	331.3	24.88
	Min.	0.6	1.4	1.1	0.04
	Average	3.61	16.15	42	5.77

4.5. Suitability of intermediate zone for ceramic industry

Pegmatites represent one of main sources of several industrial minerals, such as quartz, kaolin, and feldspars. The chemical compositions of the studied K-feldspar from El-Dob pegmatite body were compared with the standard chemical composition of the feldspar raw material used in ceramic industry materials by Ceramica Cleopatra Company (Personal communication). The contents of major oxides in the intermediate zone (i.e. K-feldspar) from El-Dob pegmatite body fall within the ranges of the standard values for the material used in ceramic industry (Table 2). There are many tests were done for feldspar to adapt the quality of feldspars for ceramic industry. These physical tests include, shrinkage, water absorption and bending strength according to international standard limit (Konta, 1980). These physical tests were applied on the prepared green biscuit ceramic sample (Table 3)., where each ceramic sample was dried and fired, then the shrinkage testing was carried out using Vernier caliper 150 x 0.05 mm. Shrinkage is directly proportional to total alkali content and inversely proportional with water absorption and bending strength. Finally, the water absorption was measured for each sample. The comparison of the obtained results of physical tests on the samples from intermediate zone with the standard values indicates that the tested green and fired ceramics, prepared from Wadi El-Dob area fit well with wall ceramic tiles rather than floor ceramics tile (Table 3).

5. Radiometric investigation

For performing field radiometric investigation to studied pegmatite plugs, detailed grid pattern of radiometric surveying was integrated to determine distribution and concentrations of radioactive elements include Potassium isotope in weight percent (40K%), equivalent U (eU), and equivalent Th (eTh) content in (ppm) in wadi El Dob pegmatites. About 110 stations within unequal twelve profiles delineated to cover an area of 120 m^2 and bounded by boundary of pegmatite plugs (Fig.10). These profiles trending N-S with in-between spacing ten meters were delineated and measured to determine 40K%, eU (ppm) and eTh (ppm) contents for the study pegmatites. In addition, maximum, minimum and estimated averages, together with eTh/eU ratios of measurements are presented in table (4). Moreover, the average contents of the radioactive elements eU and eTh and eTh/eU ratio for studied pegmatites and for that published by Rogers & Adams (1969); Clarck et al. (1966); Turkian & Wedepohl (1961) are given in table (5) for comparison.

5.1. Distribution of 40K, eU and eTh in the studied pegmatite

In the studied pegmatites as general, by referring to the detected values in ground radiometric surveying, several measurements have high content of 40K, eU and eTh regarding content of the semi clan of rock types from same radioactive element. It is obvious that the content of 40K % (0.6 - 6.9 %; average 3.61 %) m while the eU contents (1.4 - 161.3 ppm; average 16.15 ppm) which is more than that of the granites displayed (e.g. El Gharbawy et al., 2012; El-Nahas, 2012: Sallam et al., 2019). The uranium content and concentration in the pegmatites generally considered acceptable value with exception of 14 measurements which have values more than 19.7 ppm. On the other hand, equivalent Th contents in the studied samples are (1.1 - 331.3 ppm; average 42 ppm). This average is more than the average content of equivalent thorium displayed for the granites, for granitic rocks and for low Ca-granites and for the acidic intrusive. In detail, the 78 measurements have values more than the highest thorium content displayed for acidic intrusive. Only 22 measurements compatible with acceptable content of thorium make the feldspar raw material fit to using in ceramic industry.

Normally, Th is three times as abundant as U in granitic rocks (Roger and Adams, 1969). The Th/U ratio should remain constant during magmatic fractionation. As this ratio is disturbed, this leads to a U depletion and/or enrichment.

In the present study, The eTh/eU ratio ranges between 0.04 and 24.88 with an average 5.77. The eTh/eU ratio for present rock is more than that displayed for the granites, but nearly compatible with eTh/eU average ratios displayed for low Ca-granites and acidic intrusive displayed. The ratio values are relatively high in most of the measurements. This indicates that the radioactive minerals responsible for these anomalies are Th-rich rather than U-rich. This behaviour may indicate the presence of secondary post magmatic processes affecting the distributions of uranium and thorium within the studied pegmatites. These phenomena controlled by ascending and/or descending solutions effects and their pass way through joints, fractures, and faulting zone. Also, the obtained data indicate that the radioactivity of this pegmatites rock is due to the presence of some accessory minerals detected within the pegmatites and surrounding granites. These minerals include zircon, apatite, xenotime, monazite, sphene, allanite, fluorite, and biotite along with Fe -Ti oxides. These accessory minerals are considered the important hosted mineral for uranium and/or thorium cations. Also, the radioactive elements are adsorbed on the crystals surface of some altered hydrated minerals specially amphibole, mica, and clay minerals. All these minerals are responsible for the radioactivity in pegmatites. When considering the environmental risk, the sites of high radioactive value should be excluded from feldspar quarry. These anomalous feldspars are not favored for ceramic and architectural industries as well as construction fields. The environmental hazard of these anomalous feldspars arises from direct exposure to radiation emitted from potassium 40, uranium and thorium. For better understanding of the relationships between eU and eTh on one hand and the relation between eTh and eU versus eTh/eU on the other hand, these parameters are graphically represented in figure (11). For obtaining an expressive graphical correlation between eTh and eU, the odd high values of the two radioelements (nine eU and seven eTh) must be (Fig.11b & c). Figure (11b) presents the plotting of eU versus eTh/eU where a negative correlation exists whereas the plotting of eTh versus eTh/eU (Fig. 10c) shows a positive correlation. These reveals a post-magmatic remobilization process affected the behaviour of the two radioelements excluded. The binary variation diagram of eU and eTh contents of pegmatite (Fig.11a), shows an obvious negative correlation between them. This result confirms the effects of the post magmatic processes on their distribution and uranium enrichment process is also expected. However, the magmatic control on their distribution is neglected. This could indicate redistribution of uranium (Maurice, 1982). The plotting of both eTh and eU versus eTh/eU ratios of the studied pegmatites are given on the X-Y diagrams.

6. Concluding remarks

Wadi El-Dob pegmatite bodies located in the northern Eastern Desert at latitudes 26^{o} 44` 59``N and longitudes 33$^{o}$ 25` 52`` E. They are hosted by alkali-feldspar granites. The zoned pegmatite bodies consist of three successive zones; border zone which is the outer zone and occurs as fine grained with aplitic texture, intermediate zone, which consists mainly of blocky feldspars and core zone, which consists of milky quartz.

The country alkali-feldspar granites consist mainly of K- feldspars, quartz, and plagioclase with rare biotite. Muscovite and chlorite after biotite are found as secondary minerals. Allanite, sphene, zircon, monazite, apatite, and iron oxides are accessory minerals. The studied pegmatites are pinkish in color and displays coarse-grained and hypidiomorphic texture. The border zone is consisting mainly of plagioclase, quartz, muscovite, and rare K-feldspar with subordinate amounts of fluorite and topaz. The intermediate zone composed mainly of perthite, quartz and muscovite while the core zone consists mainly of quartz, muscovite and cassiterite. The heavy minerals separation detected hematite, rutile, zircon, pyrite, cassiterite, columbite-tantalite and xenotime minerals. The presence of ferrugination process (i.e. hematite) and goethite may indicate that iron has been derived from the iron-rich fluids (iron-hydrothermal solutions) rather than oxidizing both ferromagnesian mineral silicates and in magnetite (El-Desoky, 2018). Rutile formed as a result of the partial alteration of ilmenite, that indicating a post-magmatic alteration process. The presence of columbite-tantalite, cassiterite, xenotime and fluorite as a source of Nb, Sn, Y and F respectively indicating that the pegmatite body of Wadi El-Dob is NYF-type. NYF pegmatites are interpreted as deriving from mantle-sourced anorogenic magmas with a peralkaline signature (Estrade et al., 2001; Schmitt et al., 2022). NYF, garnet-REE pegmatite containing ilmenite and Nb-Ta minerals should originate as the product of melt segregation within the granite during its crystallization (Bonzi et al., 2021; 2023).

Fluid inclusions petrography recoded the following types: Primary inclusions include two subtypes, which are: a) subtype 1a: Two phase (L+V) aqueous inclusions; b) subtype 1b: Three phases (H_2O liquid + CO_2 liquid + CO_2 vapor) inclusions.

Generally, the immiscibility supercritical CO_2 fluid and liquid rich in H_2O coexist in many environments of the shallow crust (Kaszuba et al., 2006). The occurrence of two-phase aqueous, and three phase (H_2O-CO_2) inclusions could be due to partial immiscibility of one homogeneous fluid (H_2O-CO_2-NaCl) or due to mixing of two inhomogeneous fluids (Ramboz et al., 1982). There is similarity in microthermometric results between both types of inclusions.

The two- phase (L+V) aqueous inclusions (stage I) have low salinity (4.6 wt. %) and low homogenization temperature (190-270 ^{o}C). The three-phase (H_2O-CO_2) inclusions (stage II) have high salinity (11.5 wt. %) and high homogenization temperature (170 - 450 ^{o}C). The poly- phase inclusions were entrapped during the hydrothermal stage. The temperatures of homogenization show a wide range from 170 ^{o}C to 340 ^{o}C that may be due to simple cooling. At 4000 bars pressure of trapping the estimated temperature from isochors range between 170 ^{o}C and 450 ^{o}C is. The fluids of both stage I and II may be derived from a magmatic source, most likely and 3) the similarity in microthermometric results between both types of inclusions. The pressure of trapping estimated from isochors at temperature between 170^{o} and 340^{o}C are 139 and 2330 bars. two- phase (L+V) aqueous inclusions.

Geochemically, the concentrations of SiO_2 and Na_2O of Wadi El-Dob increase from intermediate zone through associated granites to border zone. In contrast, the

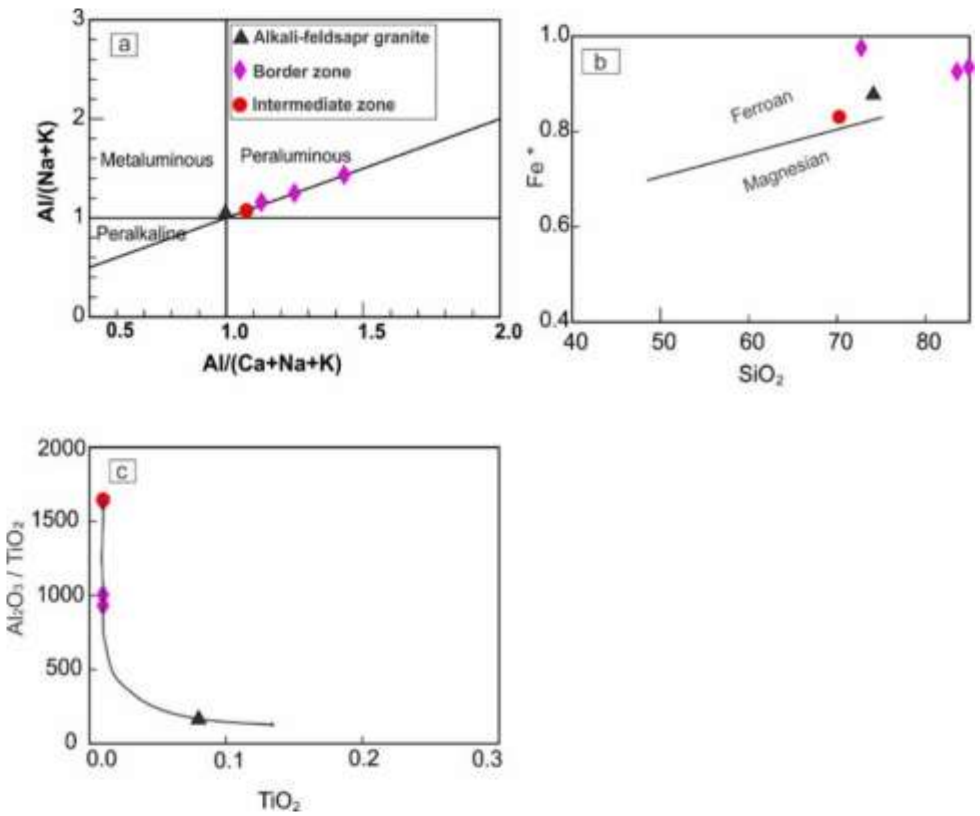

Fig. 9. a) Plot of molar Al_2O_3/ (Na_2O+ K_2O) versus Al_2O_3/ (Na_2O+ K_2O+ CaO) diagram (Shand, 1947); b) SiO_2- Fe* (FeO $_{to}$t/ FeO $_{tot}$ + MgO) diagram (Frost and Frost, 2008); c) TiO_2- (Al_2O_3/TiO_2) diagram.

Fig. 10. Landsat TM-image, showing delineated boundary of ground radiometric surveying area in Wadi El Dob pegmatite bodies, South Central Eastern Desert, Egypt.

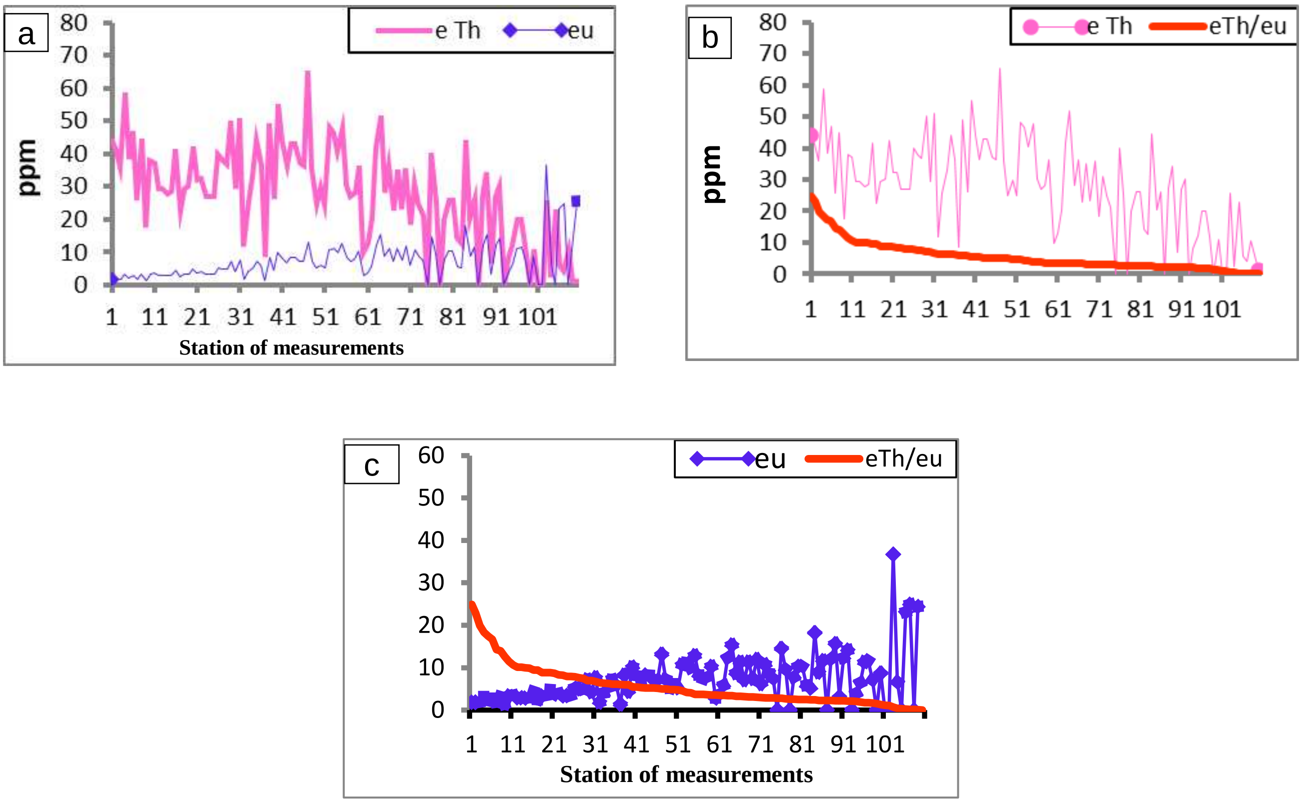

Fig. 11. (a-c). Radioactive elements plot of ground gamma-ray spectrometry measurements for the studied pegmatites, a) eTh versus eU; b) eTh versus eU/eTh; c) eU versus eU/eTh.

devolatilizing of the associated alkali-feldspar granites. Secondary inclusions are represented mainly by liquid rich two-phase aqueous inclusions in association with poly-phase (L+V+S) inclusions and mono-phase inclusions. The coexisting of two-phase aqueous, and three-phase inclusions in Wadi El-Dob pegmatite body, is interpreted as due to partial immiscibility of one homogeneous fluid

(H_2O-CO_2-NaCl) for the following reasons: 1) the presence of H_2O-rich and CO_2-rich inclusions, 2) the occurrences of two fluid inclusion types in the same region of the same samples (Chi et al., 2021), Al_2O_3 and K_2O contents increase from wall zone through granitic rocks to intermediate zone. On the other hand, the wall zone and intermediate zone are depleted in TiO_2, Fe_2O_3, MgO and CaO relative associated granites.

Generally, pegmatites are commonly interpreted to have formed from residual melts derived from crystallizing granitic plutons (e.g. Černý, 1991a; Černý & Ercit, 2005; London, 2008), this applicable especially for pegmatites that are hosted within the parental pluton (e.g. Thomas & Davidson, 2016; Roda-Robles et al., 2018). The studied alkali-feldspar granites and pegmatites were derived from a peraluminous magma. Furthermore, both samples from alkali-feldspar granites and pegmatites reveal a typical of magmatic differentiation, which is compatible with the fractional crystallization model (Garcia et al., 1994). According to the rutile saturation equation the temperatures of crystallization of the border zone in the studied pegmatite range from 560 °C to 570 °C.

The chemical compositions of intermediate zone (K-feldspar) from El-Dob pegmatites fall within the ranges of the standard raw material used from ceramic industry. On the other hand, the tested green and fired ceramics, prepared from Wadi El Dob area fit well with the standard values of wall rather than floor ceramics tiles.

Distribution and concentration of ^{40}K, uranium and thorium elements have discrepancy from low, normal up to high measurements value. This discrepancy is interpreted as a result of the effect of post-magmatic processes. Environmentally, the sites of high radioactive measurement values should be excluded from feldspar quarry due to high risk of direct radiation exposure.

Ethics approval and consent to participate: This article does not contain any studies of human participants or animals performed by any of the authors.

Consent for publication: All authors declare their consent for publication.

Funding: Self-funding

Conflicts of Interest: The author declares no conflict of interest.

Contribution of Authors: All authors shared in writing, editing, and revising the MS and agreed to its publication.

Acknowledgement: The authors would like to a great thanks to the reviewers for their help in improving the manuscript.

References

Abd El Monsef M, Sami M, Toksoy-Köksal F, et al. (2023): Role of Magmatism and Related-Exsolved Fluids during Ta-Nb-Sn Concentration in the Central Eastern Desert of Egypt: Evidence from Mineral Chemistry and Fluid Inclusions. J. Earth Scie 34 (3): 674-689, https://doi.org/10.1007/s12583-022-1778-y

Abu Elatta SA (2019): Geology, mineralogy and mineral chemistry of the NYF-type pegmatites at the Gabal El Faliq area, South Eastern Desert, Egypt. J Earth System Scie 128-156, https://doi.org/10.1007/s12040-019-1169-7

Adams JAS., Osmand JK, Rogers JJW (1956): The geochemistry of thorium and uranium In: Physics and chemistry of the Earth, 3: 298-348, Pergamon Press, New York.

Bodnar RJ (1993): Revised equation and table for determining the freezing point depression of H_2O-NaCI solutions. Geochim Cosmochim Acta, 57 (3): 683-684,https://doi.org/10.1016/0016-7037(93)90378-A

Bonzi WM-E, Vanderhaeghe O, Van Lichtervelde M, Wenmenga U, André-Mayer A-S, Salvi S, Poujol M (2021): Petrogenetic links between rare metal-bearing pegmatites and TTG gneisses in the West African Craton: the Mangodara district of SW Burkina Faso. Precambrian Res 364:106359. https://doi.org/10.1016/j. preca mres. 2021.106359

Bonzi WM-E, Vanderhaeghe O, Van Lichtervelde M, Wenmenga U, André-Mayer A-S, Salvi S, Wenmenga U (2023): Insights from mineral trace chemistry on the origin of NYF and mixed LCT + NYF pegmatites and their mineralization at Mangodara, SW Burkina Faso. Mineralium

Deposita58:75-104, https://doi.org/10.1007/s00126-022-01127-x

Borisenko AS (1997): Study of the salt composition of solutions in gas-liquid inclusions in minerals by the cryometric method. Soviet Geol Geophys 18: 11-19. (In Russian).

Bowers, TS, Helgeson HC (1983): Calculation of the thermodynamic and geochemical consequences of nonideal mixing in the system H_2O-CO_2-NaCl on phase-relations in geologic systems - Metamorphic equilibria at high-pressures and temperatures. Am Mineral 68 (11-12): 1059-1075.

Brown PE (1989): FLINCOR: A Microcomputer Program for the Reduction and Investigation of Fluid Inclusion Data. Am Mineral 74 (11): 1390-1393.

Černy P (1982): Petrogenesis of granitic pegmatites. In: Černy P (ed.): Granite pegmatites in Science and Industry Mineral Assoc Canada Short course 8, 461p.

Černý P (1991a): Rare-element granitic pegmatites. Part I: anatomy and internal evolution of pegmatitic deposits. Geosci Can 18 (2): 49-67.

Černý P (1991b): Rare-element granitic pegmatites. Part II: Regional to global environments and petrogenesis. Geosci Can 18 (2): 68-81.

Černý P, Ercit TS (2005): Classification of granitic pegmatites revisited. Can. Mineral. 43: 2005–2026.

Chi G, Diamond LW, Lu H, Lai J, Chu H (2021): Common Problems and Pitfalls in Fluid Inclusion Study: A Review and Discussion. Minerals, 11: 7, https://dx.doi.org/10.3390/min11010007

Clark SP Jr, Peterman ZE, Heier KS (1966): Abundance of uranium, thorium, and potassium. In: Clark SP (ed.), Handbook of Physical Constants. Geol Soc Am Mem 97 (24): 521-541.

Collins PLF (1979): Gas hydrates in CO_2-bearing fluid inclusions and the use of freezing data for estimation of salinity. Econ Geol 74 (6): 1435-1444, https://doi.org/10.2113/gsecongeo.74.6.1435

Crawford ML, (1981): Phase equilibria in aqueous fluid inclusions. In: Hollisten LS, & Crawford ML (eds.) Short Course in Fluid Inclusions: Applications to Petrology 6, Min Assoc Canada. 157-181.

Diamond LW (1992): Stability of CO_2-clathrate-hydrate + CO_2 liquid +CO_2 vapour + aqueous KCl-NaCl solutions: Experimental determination and application to salinity estimates of fluid inclusion. Geochim Cosmochim Acta 56 (1): 273-280, https://doi.org/10.1016/0016-7037(92)90132-3

El Gharbawy RI, El Maadawy WM (2012): Geochemistry of the uranium-thurium-bearing granitic rocks and pegmatites of Wadi Haleifiya area, Southeastern Sinai, Egypt. Chin J Geochem 31: 242–259, https://doi.org/10.1007/s11631-012-0573-3

El Nahas HA (2012): Mineralogy and radioactivity of some pegmatite bodies, southeastern Sinai, Egypt. Nucl Sci Scient J 1 (1): 57-68, HTTPS://doi.org/10.21608/nssj.2012.31020

El- Shazly EM, Abdel Hady MA, El-Ghawaby MA, El-Kassas IA, El-Shazly MM (1974): Geology of Sinai Peninsula from ERTS-1 satellite images, Remote Sensing Research project, Academy of Sciences Research and Technology, Cairo, Egypt. 20p.

El-Desoky HMA (2018): Late Cryogenian–Ediacaran Crustally-Derived Granites in El-Qasia Region, Central Eastern Desert, Egypt: Constraints from Geochemistry and Hydrothermal Alteration Mineralogy. Annals Geol Surv Egypt XXXV, 61- 91.

El-Nahas HA (1997): Geochemistry and mineralogy of some radioactive pegmatites, Abu Zawal area, Easten Desert, Egypt. MSc. Thesis, Faculty Science, Menofiya University, Egypt 140p.

Estrade G, Salvi S, Béziat D, Rakotovao S, Rakotondrazafy R (2014): REE and HFSE mineralization in peralkaline granites of the Ambohimirahavavy alkaline complex, Ampasindava peninsula, Madagascar. J Afr Earth Sci 94: 141-155, https://doi.org/10.1016/j.jafre arsci.2013.06.008

Fawzy, M. M., Mahdy NM, Sami M (2020): Mineralogical characterization and physical upgrading of radioactive and rare metal minerals from Wadi Al-Baroud granitic pegmatite at the Central Eastern Desert of Egypt. Arab J Geosci 13 (11): 413, https://doi.org/10.1007/s12517-020-05381-z.

Garcia D, Fonteilles M, Moutte J (1994): Sedimentary fractionation between Al, Ti, and Zr and the genesis of strongly peraluminous granites. J Geol 102 (4): 411- 422, https://doi.org/10.1086/629683

Greenberg J K (1981): Characteristics and origin of Egyptian younger granites. Geol Soc Amer Bul 11 (92): 224-232.

Hayden LA, Watson EB (2007): Rutile saturation in hydrous siliceous melts and its bearing on Ti-thermometry of quartz and zircon. Earth Planet Sci Lett 258 (3- 4): 561-568, https://doi.org/10.1016/j.epsl.2007.04.020

Helmy HM (1999). Mineralogy, Fluid inclusions and geochemistry of the molybdenum-uranium-fluorite mineralizations, Gebel Gattar Area, Eastern Desert, Egypt. 4th Inter Conf. Geochem Alexandria University 1: 171-188.

Hollister LS, Crawford ML (1981): Fluid Inclusions-Applications in Petrology; Mineralogical Association of Canada Publications: Québec, QC, Canada 6, 304 p.

Kaszuba JP, Williams LL, Janecky DR, Hollis WK, Tsimpanogiannis IN (2006): Immiscible CO_2-H_2O fluids in the shallow crust. Geochem Geophy Geosyst 7 (10): 1-11, https://doi.org/10.1029/2005GC001107

Khaleal FM (2014): Granites of Gabal El-Dob area and associated pegmatites, Central Eastern Desert, Egypt: Geochemistry and spectrometry. Nucl Sci Scient J 3(1):15-25, https://doi.org/10.21608/nssj.2014.30936

Khaleal FM, Saleh GM, Lasheen ESR, Alzahrani AM and Kamh SZ (2022): Exploration and Petrogenesis of Corundum-Bearing Pegmatites: A Case Study in

Migif-Hafafit Area, Egypt. Front. Earth Sci. 10, 869-828, https://doi.org/10.3389/feart.2022.869828

Konta J (1980): Properties of Ceramic Raw Materials" Ceramic Monographs- Handbook of Ceramics. Verlag Schimd GmbH Freiburg.

London D (2008): Pegmatites. Can Mineral Spec Publ, 10, 347 p., https://doi.org/10.2138/am.2009.546

Maurice YT (1982): Uranium in granites. Geological Survey of Canada 81 (23):167-168.

Pal DC, Mishra B, Bernhardt H-J (2007): Mineralogy and geochemistry of pegmatite-hosted Sn-, Ta–Nb-, and Zr–Hf-bearing minerals from the southeastern part of the Bastar-Malkangiri pegmatite belt, Central India. Ore Geol Rev 30 (1): 30-55, https://doi.org/10.1016/j.oregeorev.2005.10.004

Poty B, Leroy J, Jakimowicz L (1976): Un nouvel appareil pour la mesure des temperatures sous le microscope: l`Installation de microthermometrie Chaixmeca. Bulletin de la Societe francaise de Mineralogie et Cristallographie 99: 182-186.

Ramboz C, Pichavant M, Weisbrod A (1982): Fluid immiscibility in natural processes: Use and misuse of fluid inclusion data II. Interpretation of fluid inclusion data in terms of immiscibility. Chem Geol 37 (1-2): 29-48, https://doi.org/10.1016/0009-2541(82)90065-1

Rashwan AA (1991): Petrography, geochemistry and petrogenesis of the Migif-Hafafit gneisses at Hafafit mine area, South Eastem Desert, Egypt. Sci Ser Intem Barea 5: Forschangszentran Julich GmbH, 359 p.

Raslan MF, Ali MA (2011): Mineralogy and mineral chemistry of rare-metal pegmatites at Abu Rusheid granitic gneisses, South Eastern Desert, Egypt. Geologija 54/2: 205-222, http://dx.doi.org/10.5474/geologija.2011.016

Raslan MF, El-Shall HE, Omar SA, Daher AM (2010a): Mineralogy of polymetallic mineralized pegmatite of Ras Baroud granite, Central Eastern Desert, Egypt J Mineral Petrol Scie 105 (3): 123-134, https://doi.org/10.2465/jmps.090201

Raslan, M.F., Ali, M.A., and El Feky, M.G., 2010b. Mineralogy and radioactivity of pegmatites from South Wadi Khuda area, Eastern Desert, Egypt. Chin J Geochem 29: 34-354, https://doi.org/10.1007/s11631-010-0466-2

Roda-Robles E, Villaseca C, Pesquera A, Gil-Crespo PP, Vieira R, Lima A, Garate-Olave I (2018): Petrogenetic relationships between Variscan granitoids and Li-(F-P)-rich aplite-pegmatites in the Central Iberian Zone: Geological and geochemical constraints and implications for other regions from the European Variscides. Ore Geol Rev 95:408–430, https://doi.org/10.1016/j.oregeorev.2018.02.027

Roedder E (1979): Fluid inclusions as samples of ore fluids. In Barnes HL (ed.), Geochemistry of Hydrothermal Ore Deposits, 2nd ed. Wiley, New York: 684-737.

Roedder E (1984): Fluid Inclusions, Min Soc Am Series Review in Mineralogy and Geochemistry 12: 644 p., https://doi.org/10.1515/9781501508271

Rogers JJ, Adams JSS. (1969): Uranium. In: Wedepohl KH (ed.), Handbook of Geochemistry, Springer-Verlag, Berlin, 2 (I), Chap.12, 50p.

Ryerson FJ, Watson EB (1987): Rutile saturation in magmas: implications for Ti-Nb-Ta depletion in island-arc basalts. Earth Planet Sci Lett 86 (2-4): 225-239, https://doi.org/10.1016/0012-821X(87)90223-8

Sallam OR, Alshami AS, Abbas AE (2019): Geology and mineralogy of a radioactive pegmatite body at Wadi Zaghra area, southeastern Sinai, southeastern Sinai, Egypt. Nucl. Sci. Scient. J 8(A): 191- 205.

Saleh, G.M., 2007. Rare metal-bearing pegmatites from the south-eastern desert of Egypt: Geology, geochemical characteristics, and petrogenesis. Chin J Geochem 26 (1), https://doi.org/10.1007/s11631-007-0008-8

Satterly J (1957): Radioactive mineral resources in the Bancroft Area: Ontario Department of Mines Annual Rep 65 (6): 181p.

Schmitt AK, Trumbull RB, Dulski P, Emmermann R (2002): Zr-Nb-REE mineralization in peralkaline granites from the Amis Complex, Brandberg (Namibia): evidence for magmatic pre-enrichment from melt inclusions. Econ Geol 97 (2):399-413, https://doi.org/10.2113/gsecongeo.97.2.399

Shalaby MH, Salman AB, El Kammar AM, Mahdy AI (1999): Uranium mineralization in the Hammamat sediments of the Gattar area, Northeasten Desert, Egypt. 4th Inter Conf Geochem Alexandria University, Egypt, 101-121.

Shand SJ (1947): Eruptive Rocks: Their Genesis, Composition, Classification and their Relation to Ore Deposits, 3rd ed. John Wiley and Sons, 448 p.

Shepherd TJ, Rankin AH, Alderton DHM (1985): A practical Guide to Fluid Inclusion Studies. Blackie Academic & Professional (an Imprint of Chapman & Hall, 224p. ISBN-13: 978-0216916463

Simmons WB, Hanson SL, Falster AU (2006): Samarskite-Yb: a new species of the samarskite group from the Little Pasty pegmatites, Jefferson County, Colorado. Can Mineral 44 (5), 119-1125.

Streckeisen A, Le Maitre RW (1979): A chemical approximation to the modal QAPF classification of the igneous rocks. Neues Jahrb Mineral Abh 136: 169-206.

Thomas R, Davidson P (2016): Origin of miarolitic pegmatites in the Königshain granite/Lusatia. Lithos 260:225-241, https://doi.org/10.1016/j.lithos.2016.05.015

Turekian KK, Wedephol KH (1961): Distribution of elements in some major units of Earth’s crust. Geol Soc Am Bull 72 (2): 175-190, https://doi.org/10.1130/0016-7606(1961)72[175:DOTEIS]2.0.CO;2

Vasyukova OV, Williams-Jones AE (2019): Closed system fluid-mineral mediated trace element behaviour in peralkaline rare metal pegmatites: Evidence from Strange Lake. Chem Geol 505: 86-99, https://doi.org/10.1016/j.chemgeo.2018.12.023

Zhang Y, Frantz D (1987): Determination of the homogenization temperatures and densities of supercritical fluids in the system $NaClKClCaCl_2H_2O$ using synthetic fluid inclusions. Chemical Geology, 64, 335-350, https://doi.org/10.1016/0009-2541(87)90012-X

دراسات معدنية ومكتنفات الموائع وإشعاعية على بجماتيت وادي الدب شمال الصحراء الشرقية، مصر

وحيد علوان[١]، وأحمد دردير[٢]، وإسماعيل أحمد العقيد[٢]، وعماد خليل[١]، وهدير صبحي[١]

[١] قسم الجيولوجيا- كلية العلوم- جامعة الزقازيق - الزقازيق-٤٤٥١٩- مصر

[٢] هيئة المواد النووية، ص.ب: ٥٣٠ المعادي، القاهرة، مصر

يقع بيجماتيت وادي الدب في شمال الصحراء الشرقية، يتكون جسم البجماتيت من ثلاث نطاقات متتالية: النطاق الحدودي والنطاق الوسيط ونطاق اللب . يوجد البجماتيت داخل جرانيت الفلسبار القلوي ويحتوي على معادن مثل البلاجيوجلاز، الكوارتز، الموسكوفيت، الفلسبار البوتاسى, الفلوريت، التوباز، الهيماتيت، الروتيل، البيريت، الكاستيريت، الكولومبيت - تانتاليت والزينوتيم. تشير هذه التجمعات المعدنية إلى أن بجماتيت وادى الدب يمكن تصنيفه على أنه بيغماتيت من نوع (NYF). كشفت دراسات مكتنفات الموائع عن وجود ثلاثة أنواع من المكتنفات وهى: مكتنف موائع مائي ثنائي الطور، ومكتنف موائع ثلاثي الطور، ومكتنف متعدد الطور. أظهر النوع الأول (المرحلة الأولى) درجة حرارة تجانس وملوحة منخفضة نسبيا، بينما أظهر النوع الثاني (المرحلة الثانية) ودرجة حرارة تجانس وملوحة عالية مقارنة بالنوع الاول. تشكلت مكتنفات موائع متعددة الطور خلال المرحلة الحرارية المائية. يمكن أن يعزى نطاق درجة حرارة التجانس الواسع لمكتنفات الموائع إلى عملية التبريد البسيط. تتفاوت درجات الحرارة المقدرة من الأيزوكورات ما بين النطاق السفلي والعلوي تحت ضغط معين. من المحتمل أن تكون مكتنفات موائع المرحلتين الأولى والثانية قد نشأتا من مصدر مجماتى وربما يرتبط تكوين هذه المكتنفات بفقدان المكونات المتطايرة من جرانيت الفلسبارالبوتاسى. يمكن تفسير التصاحب بين أنواع مختلفة من مكتنفات الموائع إلى عدم الامتزاج الجزئي لسائل متجانس (H_2O-CO_2-NaCl) وذلك بسبب وجود مكتنفات موائع غنية بالماء وغنية بثاني أكسيد الكربون ، وايضا بسبب تواجد هذه المكتنفات في نفس المنطقة ونفس العينات وتماثل قياسات الحرارية الدقيقة لهذه المكتنفات. يعتقد عموما ان البجماتيت قد تبلرت من صهير جرانيتى، وخاصة تللك البجماتيت المستضافة داخل المصدر الجرانيتى. جيوكيميائيا, يشير تشابه نوع الصهارة بين الجرانيت القلوي الفلسبار وجسم البجماتيت المصاحب له إلى مصدر مشترك للصهارة. حيث تظهر عينات كل من الجرانيت والبجماتيت اتجاها نموذجيا للتمايز الصهيرى, بما يتفق مع عملية التبلور الجزئي. والتالى من المحتمل أن يكون جسم البجماتيت مشتقا من ذوبان الجرانيت. البجماتيت من نوع (NYF) الخالية من معدن الجارنت والتى تحتوي على معدن الإلمينيت ممكن أن تنشأ كمنتج من تمايز الصهير داخل الجرانيت خلال تبلوره. علاوة على ذلك, يتم ارجاع البجماتيت من نوع (NYF) على أنها مشتقة من الصهارة المولدة من مصدر من الوشاح مع اثر فوق قلوى. شهدت المنطقة الحدودية للبيجماتيت درجات حرارة تبلور تتراوح بين ٥٦٠ إلى ٥٧٠ درجة مئوية. التركيب الكيميائي للفلسبار من وادي الدب والاختبارات الفيزيائية التي أجريت على السيراميك المصنوع من عينات البجماتيت تشير إلى ملاءمتها لصناعة بلاط السيراميك الجداري وفقا للقيم القياسية. كشفت القياسات الإشعاعية الميدانية لبيجماتيت الدب عن محتوى متفاوت من اليورانيوم, والثوريوم. وتشير هذه الاختلافات إلى حدوث عمليات حرمائية ومجماتية، مما يشير إلى حدوث عمليات بعد ماجماتية مؤثرة. وبالتالي يوصى باستبعاد عينات بجماتيت وادى الدب ذات القيم الاشعاعية العالية من الاستخدام في صناعة السيراميك.